

Mechanisms of acute axonal degeneration in the optic nerve in vivo

Johanna Knöferle^{a,1}, Jan C. Koch^{a,1}, Thomas Ostendorf^a, Uwe Michel^a, Véronique Planchamp^a, Polyva Vutova^a, Lars Tönges^a, Christine Stadelmann^{b,c}, Wolfgang Brück^{b,c}, Mathias Bähr^{a,c}, and Paul Lingor^{a,c,2}

Departments of ^aNeurology and ^bNeuropathology, University Medicine, Georg-August University, 37075 Göttingen, Germany; and ^cDeutsche Forschungsgemeinschaft Research Center for Molecular Physiology of the Brain, 37075 Göttingen, Germany

Edited by Jeremy Nathans, Johns Hopkins University, Baltimore, MD, and approved February 17, 2010 (received for review August 28, 2009)

Axonal degeneration is an initial key step in traumatic and neurodegenerative CNS disorders. We established a unique in vivo epifluorescence imaging paradigm to characterize very early events in axonal degeneration in the rat optic nerve. Single retinal ganglion cell axons were visualized by AAV-mediated expression of dsRed and this allowed the quantification of postlesional acute axonal degeneration (AAD). EM analysis revealed severe structural alterations of the cytoskeleton, cytoplasmatic vacuolization, and the appearance of autophagosomes within the first hours after lesion. Inhibition of autophagy resulted in an attenuation of acute axonal degeneration. Furthermore, a rapid increase of intraaxonal calcium levels following crush lesion could be visualized using a calcium-sensitive dye. Application of calcium channel inhibitors prevented crush-induced calcium increase and markedly attenuated axonal degeneration, whereas application of a calcium ionophore aggravated the degenerative phenotype. We finally demonstrate that increased postlesional autophagy is calcium dependent and thus mechanistically link autophagy and intraaxonal calcium levels. Both processes are proposed to be major targets for the manipulation of axonal degeneration in future therapeutic settings.

CNS trauma | live imaging | calcium influx | autophagy

Axonal degeneration plays a pivotal role in the pathogenesis of numerous neurological disorders frequently preceding neuronal cell death and resulting in persistent functional disability. Traumatic spinal cord or peripheral nerve injury represent classical conditions where mechanical disruption of axonal integrity results in nervous system dysfunction (1, 2). Several degenerative CNS diseases show prominent axonal pathology already early in the disease course, such as the degeneration of nigrostriatal projection tracts or cardiac sympathetic nerves in Parkinson's disease (3) or corticospinal tracts in amyotrophic lateral sclerosis (4). Key features of axonal degeneration seem to be similar despite variable etiology. The distal part of the lesioned axon undergoes Wallerian degeneration (WD) characterized by initial axonal stability followed by rapid degeneration, fragmentation, and blebbing of the remaining axon, microtubule disassembly, and phagocytic clearance of the lesion site. The proximal part was reported to remain more stable than its distal counterpart (5–8), but imaging of the spinal cord in vivo visualized mechanisms of acute axonal degeneration (AAD) within the first minutes after lesion. In contrast to WD, AAD results in sudden axonal disintegration and extended for ≈ 300 μm proximal and distal to the lesion (9). One of the putative initiating steps in axonal degeneration is the influx of extracellular calcium, which is suggested to destabilize the axon and to transmit apoptotic signals to the neuronal soma (10–12).

The optic nerve (ON) represents a unique model system for the study of axonal pathology in the CNS because of its accessibility and the possibility to manipulate the system via transfection of retinal ganglion cells (RGC) (13–15). Moreover, dysfunction of ON axons has clinical relevance for the pathogenesis of optic neuritis, glaucoma, Leber's optic atrophy, and trauma (16–18). In this study we present a unique epifluorescence imaging approach,

which permits the visualization of axonal degeneration in the ON of the living rat. We characterize the morphological changes following an ON crush lesion and resolve ultrastructural alterations by electron microscopy. On the basis of this characterization we link lesion-induced calcium influx to intraaxonal autophagy as major pathophysiological mechanisms contributing to acute axonal degeneration in the CNS.

Results

Visualization of Optic Nerve Axons in Vivo. To visualize single RGC axons in the ON, we injected into the vitreal space an adeno-associated viral vector (AAV, serotype 1/2) expressing the fluorescent protein dsRed (Fig. 1 *A* and *B*). Targeted injections resulted in transfection of RGC axons localized at the dorsal part of the ON (Fig. 1 *C–F*) and ~ 5 – 10 different surface-near axons per ON could be used for imaging (Fig. 1 *L* and *M*).

For imaging, the ON was exposed employing an adapted supra-orbital surgical access (Fig. 1 *A*) (19, 20) and image acquisition was performed using an upright fluorescence microscope equipped with a water-immersion objective. Due to the anatomical limits imposed by the skull this technique allowed us to image the ON in a total length of ~ 5 mm. Physiological conditioning of experimental animals under deep anesthesia with artificial respiration and temperature control permitted the acquisition of images of the live animal for up to 6 h. There was no indication of phototoxicity during this imaging period (9).

Time Course of Acute Axonal Degeneration Following Optic Nerve Crush. The ON crush is an established model for the study of CNS trauma and regeneration resulting in axonal lesion while maintaining the continuity of the nerve (21). Using a small surgical suture the ON was crushed resulting in complete transection of all axons. Due to anatomical distortion at the crush site, axonal changes could be observed only at a distance of about 150 μm from the crush site. The proximal ($n = 6$) and the distal site ($n = 5$) of the crushed axons were analyzed (Fig. 2). Axonal integrity was quantified as length ratio of the remaining axon to the appearing gaps (Fig. S14). On both sides of the lesion, the microcrush resulted in a rapid-onset, time-dependent disruption of axonal integrity: the formation of bulb-like axonal swellings started already within the first 30 min after the lesion and these structures increased in size for about 240 min, while the axon continued to disintegrate (Fig. 2 *B* and *D*). At 60 min after ON lesion, the axonal integrity ratio both proximal (0.93 ± 0.02 , $P = 0.015$) and distal (0.82 ± 0.03 , $P = 0.004$)

Author contributions: J.K., J.C.K., M.B., and P.L. designed research; J.K., J.C.K., T.O., V.P., P.V., L.T., and P.L. performed research; U.M., C.S., and W.B. contributed new reagents/analytic tools; J.K., J.C.K., T.O., P.V., and P.L. analyzed data; and J.K., J.C.K., and P.L. wrote the paper.

The authors declare no conflict of interest.

This article is a PNAS Direct Submission.

¹J.K. and J.C.K. contributed equally to this work.

²To whom correspondence should be addressed. E-mail: plingor@gwdg.de.

This article contains supporting information online at www.pnas.org/cgi/content/full/0909794107/DCSupplemental.

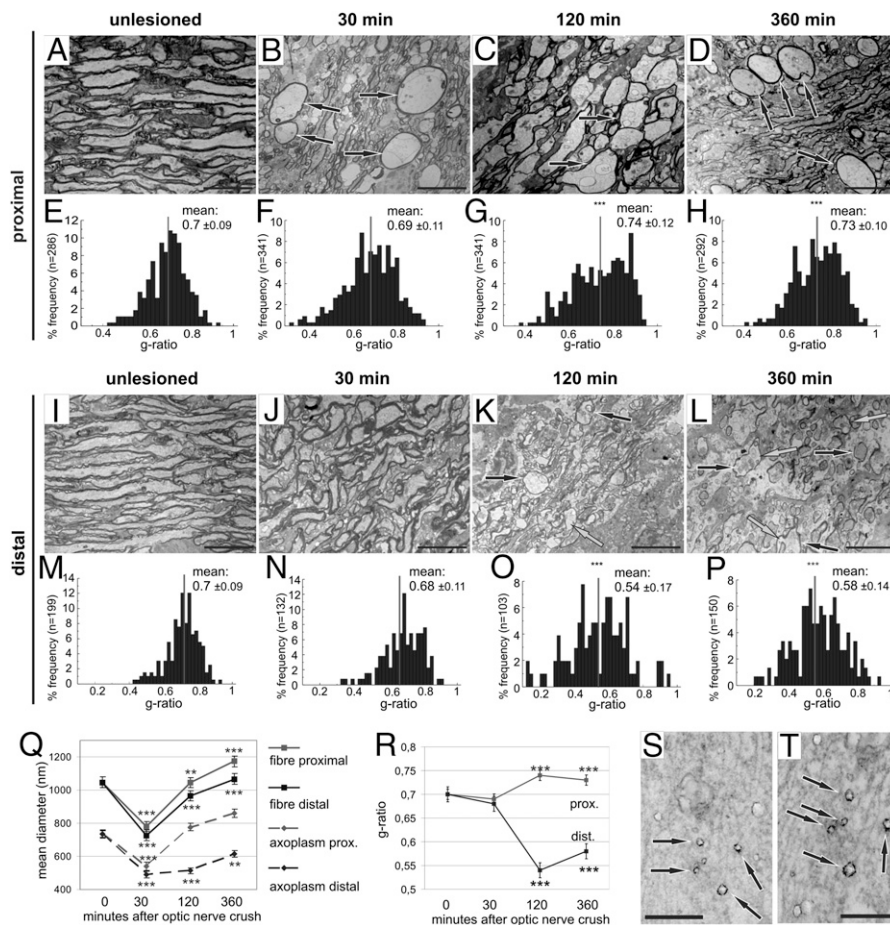


Fig. 3. Ultrastructural changes after ON crush. Overview of the ON ultrastructure in the unlesioned control ON (A and I), and 30 min (B and J), 120 min (C and K) and 360 min (D and L) after crush (all longitudinal sections). Local axonal swellings (black arrows) appear earlier proximal than distal to the crush and increase in number and size over time (A–D and I–L). Early structural defects between axoplasm and myelin sheath distal to the crush (K and L; gray arrows). Histograms of ON fibers after crush (in % frequency, bin width 0.025) (E–H and M–P). Development of the mean fiber and axoplasm diameter (Q) and the resulting g-ratio (R) over time. Mean g-ratio is given \pm SD (E–H and M–P) or \pm SEM (R). LC3-immunogold labeling for autophagosomes (black arrows) 360 min after crush (S and T). **, $P < 0.01$; ***, $P < 0.001$ (compared to unlesioned control of the corresponding side), two-tailed, heteroscedastic Student's *t* test. [Scale bars, 5 μ m (A–D and I–L); 250 nm (S); 100 nm (T).]

axons developed a marked swelling and showed structural defects between axoplasm and myelin sheath (Fig. 3 K and L), resulting in a decreased mean g-ratio and increased mean axon diameter.

Different types of local axonal swellings were identified by EM analysis (Fig. S3). The most common type was characterized by a dense cytoplasmic accumulation of organelles, mostly mitochondria and vacuoles (Fig. S3A). Mitochondria displayed structural signs of degradation, i.e., swelling, cristalline dilatation, and vacuolization (Fig. S3E). Other swellings showed a sparse axoplasm without regular structured microtubules and with only very few organelles (Fig. S3B). They extended over distances between 20 and 80 μ m along the axon and were most prevalent proximal to the crush site already at early time points of AAD (Fig. 3 B and C). Many axons were densely packed with vacuoles of different size, with mono- or bilayered membrane (Fig. S3 C and D). This type was most abundant at 360 min after crush lesion on both sides of the crush. One subpopulation of these vacuoles morphologically resembled autophagosomes and a large portion of them were positive for LC3 in immunogold labeling (360 min after crush; Fig. 3 S and T).

Crush-Induced Acute Axonal Degeneration Is Delayed by Inhibition of Autophagy. Because autophagosome accumulation was observed as a lesion-related phenomenon, we determined whether autophagy inhibition would interfere with lesion-induced axonal degeneration. A significant delay of axonal degeneration was observed at 90 min

after ON crush after application of the autophagy inhibitor 3-methyladenine (3-MA; 33.3 mM; $n = 6$; Fig. 4B) compared to control treatment (DMSO; $n = 4$; Fig. 4C). Although the degenerative process was still progressive in the 3-MA group, the axonal integrity ratio was significantly higher compared to the DMSO control even at 360 min postcrush (0.58 ± 0.05 vs. 0.2 ± 0.05 ; $P = 0.0028$; Fig. 4A). Ultrastructural alterations induced by the crush lesion were also attenuated by 3-MA application (Fig. S4).

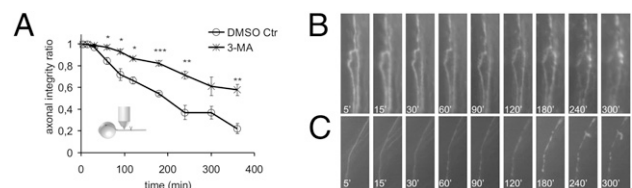


Fig. 4. Time course of axonal degeneration following autophagy inhibition by 3-MA. (A) Development of axonal integrity ratios for DMSO-treated (open rectangle; $n = 4$) and 3-MA-treated (cross; $n = 6$) animals. Error bars represent SEM. Statistical differences between DMSO- and 3-MA-treated groups: *, $P < 0.05$; **, $P < 0.01$; ***, $P < 0.001$ by ANOVA and Student's *t* test (two-tailed, heteroscedastic). Axonal changes proximal to crush at indicated time points (min after lesion) in an ON pretreated with 3-MA (B) or DMSO (C).

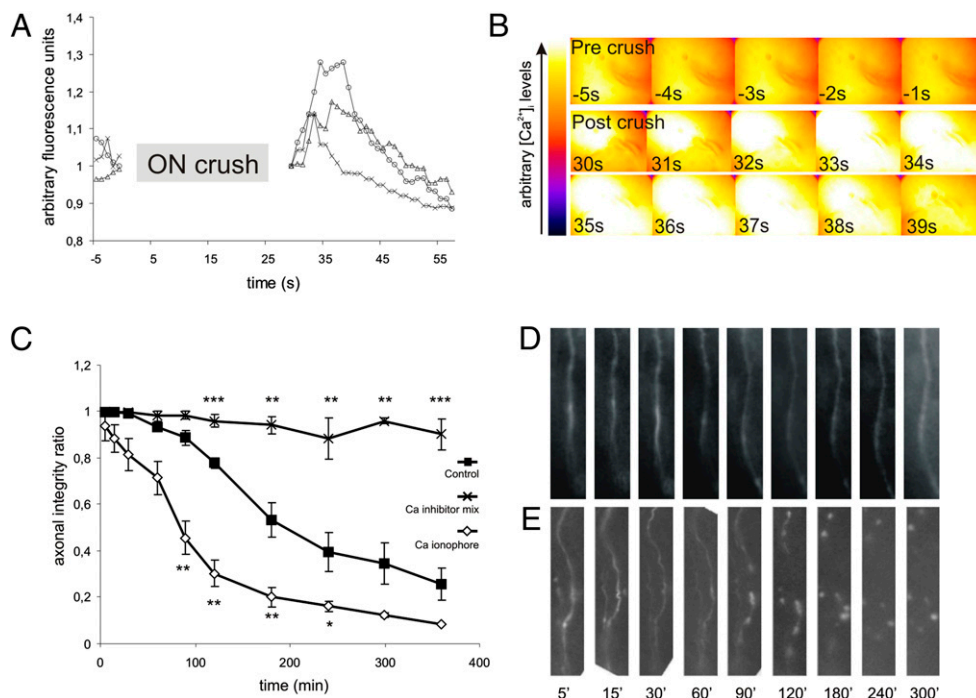


Fig. 5. Role of intraaxonal calcium levels ($[Ca^{2+}]_i$) for axonal degeneration. (A) $[Ca^{2+}]_i$ before and after ON crush in the untreated ON. Single measurements ($n = 3$). (B) Exemplary images of an ON before and after crush (crush site marked by constricted tie). Time before/after crush indicated in seconds. (C) Time course of axonal degeneration after application of a calcium channel inhibitor mixture (amiloride 100 μ M, amlodipin 10 μ M, NBQX 1 mM; crosses; $n = 5$), a calcium ionophore (A23187, 100 μ M; open rhomboids; $n = 4$), or untreated ON (control; solid squares; $n = 6$). Error bars represent SEM. Statistical differences indicated in relation to control group: *, $P < 0.05$; **, $P < 0.01$; ***, $P < 0.001$ by ANOVA and Student's t test (two-tailed, heteroscedastic). Representative images of axonal changes proximal to crush at indicated time points (min after lesion) after application of the calcium inhibitor mix (D) or the calcium ionophore (E).

Calcium Influx Following Crush Lesion. Postlesional influx of calcium has been previously proposed to be part of a series of events following traumatic axonal lesion (6, 22). However, the kinetics of intraaxonal calcium concentrations ($[Ca^{2+}]_i$) within the first seconds or minutes after CNS lesion in a living mammal so far remained enigmatic. We used the calcium-sensitive dye Oregon Green 488 BAPTA-1 (OGB-1) to follow lesion-induced changes in $[Ca^{2+}]_i$. After intravitreal injection of OGB-1, we observed anterograde labeling of the ON with an increase in fluorescence intensity reaching a maximum about 2–2.5 h after dye injection, allowing stable imaging of $[Ca^{2+}]_i$ (Fig. S5 A and B; $n = 4$). Quantification of dye bleaching showed a minimal decline in fluorescence intensity during 100 s of continuous UV exposure (6.6 \pm 2.2%; Fig. S5 C and D).

We then identified a region of interest (ROI) proximal to the tie and captured the total fluorescence in this visual field following the ON crush. The fluorescence intensity in the ROI showed a rapid increase within the first 30 s after the crush with a slow decline and normalization within the next minute ($n = 3$) (Fig. 5 A and B and Movie S1). To understand whether this increase in $[Ca^{2+}]_i$ is induced by influx of extraaxonal calcium, we applied a combination of calcium channel inhibitors (L-/N-type channel blocker amlodipine, T-type channel blocker amiloride, and AMPA receptor blocker NBQX) on the ON 30 min before ON crush. This resulted in an inhibition of the previously detected $[Ca^{2+}]_i$ increase (Fig. S5 E and F). Imaging of axonal degeneration revealed that axonal integrity ratios were highly stable in the calcium channel inhibitor group compared to untreated controls (0.96 \pm 0.03 vs. 0.78 \pm 0.03 at 120 min after crush; $P = 0.0003$; $n = 5$). This significant difference persisted during the entire imaging period with the axonal integrity ratio remaining above 0.88 at any time point (Fig. 5 C and D). However, application of the calcium ionophore A23187 aggravated degenerative dynamics. The axonal integrity ratio in the treatment

group was significantly lower compared to the untreated nerve at 90 min after crush (0.46 \pm 0.07 vs. 0.89 \pm 0.03; $P = 0.006$; $n = 4$).

Induction of Autophagy Is Mediated by Intraaxonal Calcium Levels.

To resolve the relation between the initial $[Ca^{2+}]_i$ increase and autophagy induction, we quantified the number of LC3 positive autophagosomes as well as p62 positive punctae following crush. Both proximal and distal to the crush site, the number of autophagosomes per mm^2 increased already at 30 min and was almost doubled at 360 min postcrush compared to the native ON (proximal 8,164 \pm 1,431 vs. 16,715 \pm 1,750; $P < 0.004$ and distal 6,933 \pm 1,709 vs. 14,245 \pm 2,087; $P < 0.023$; each group $n = 6$; Fig. 6). Application of the calcium inhibitor mix resulted in a significant reduction of LC3-positive autophagosomes at 360 min compared to the untreated ON at 360 min (proximal 9,078 \pm 465 vs. 16,715 \pm 1,750; $P = 0.006$ and distal 5,268 \pm 1,083 vs. 14,245 \pm 2,087; $P < 0.006$; each group $n = 6$; Fig. 6). This data demonstrates that the accumulation of autophagosomes is dependent on $[Ca^{2+}]_i$ and can be blocked by administration of Ca channel inhibitors. A similar kinetics was observed for the autophagy-related protein p62 (Fig. S6).

Discussion

Because of its structural simplicity and fast surgical accessibility, the retinotectal system is widely used as a model for the study of neuronal death, axonal de- and regeneration in the CNS (21, 23). Here we describe a unique epifluorescence imaging approach, not previously reported to the best of our knowledge, which permitted the repetitive imaging of single ON axons in the living rat.

Within the imaging period of 360 min we observed a rapid loss of integrity in axons located \sim 400 μ m to both sides of the lesion. The earliest morphological alterations were visible already in the first 30 min after lesion, which is similar to previous reports on AAD in the spinal cord (9). Axonal disintegration occurred very rapidly in the entire visualized part of the axon and this was independent of the

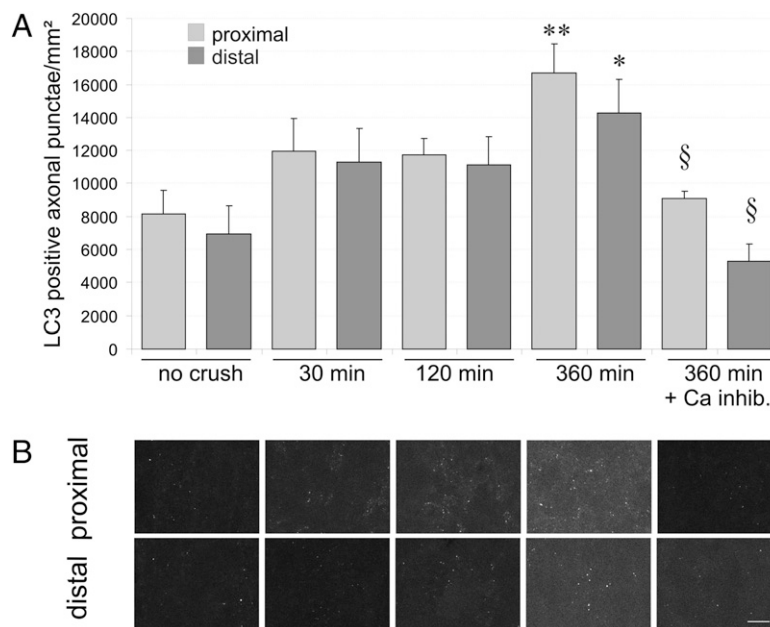


Fig. 6. Time course and Ca-dependence of autophagosome accumulation in AAD. (A) Quantification of LC3 positive axonal punctae/mm² in a native ON (no crush), in ON at 30, 120, and 360 min postcrush and at 360 min postcrush and treatment with a calcium inhibitor mix. **, $P < 0.01$; *, $P < 0.05$ vs. no crush, §, $P < 0.05$ vs. 360 min without calcium inhibitor mix. (B) Pseudoconfocal micrographs of representative areas immunostained against LC3 at 200 μ m proximal and distal to the crush corresponding to the quantification in A. (Scale bar in B, 20 μ m.)

localization of the axon to the lesion site (proximal or distal). This suggests an initially common mechanism for AAD in the vicinity of the lesion, independent of the relation to the neuronal soma (6).

Corresponding to our epifluorescence data, alterations on the ultrastructural level appeared already at 30 min after lesion. At 120 and 360 min after crush we found subtle differences between the proximal and distal side mainly in regard to the interaction of axoplasm and surrounding myelin sheath, which were inapparent by epifluorescence. The relative increase in axoplasm diameter was less sustained distal to the crush compared to proximal and resulted in a smaller distal g-ratio. This may be due to a more vital axonal transport on the proximal side leading to a faster swelling of the axoplasm. Besides, more structural defects of the myelin sheath were found distal to the crush indicating a higher vulnerability of the myelin sheath and the myelin-axolemmal contacts compared to proximal parts. Early abnormalities in neurofilament and microtubule density were described after traumatic brain injury (24) and axonal swellings with densely packed organelles, swollen mitochondria, and a vacuolization of the axoplasm were previously observed at 48 h after spinal cord lesion (25). We detected these prominent morphological features in the ON already in the early stages of AAD. Most importantly, our ultrastructural analysis revealed autophagosomes as a major component of the degenerating ON.

Autophagy regulates the homeostasis of proteins and cell organelles and has been recently linked to neurodegenerative disorders (26, 27). Purkinje cells of Lurcher mice undergoing axonal dystrophy accumulate LC3-positive autophagosomes (28). However, autophagy seems required to maintain local homeostasis of axon terminals and the ablation of the autophagy-related protein Atg7 may cause progressive dystrophy (29). We detected a persistent accumulation of autophagosomes until 6 h postcrush prompting the question of whether this mechanism participates in axonal degeneration or rather represents a homeostatic response of the axon to preserve its integrity. Inhibition of autophagy by 3-MA attenuated axonal degeneration and ultrastructural alterations, suggesting a detrimental role for autophagy in AAD.

Progressive vacuolization may be induced by the breakdown of axonal transport and local accumulation of cargo. However, axonal

transport disturbances are likely to be preceded by a lesion-induced signal, triggering ultrastructural changes and our data suggest a rapid increase in intraaxonal calcium to be such a trigger. Calcium and the calcium-binding protein calmodulin have been demonstrated to cause microtubule disassembly in vitro (30, 31). Although calcium influx has been proposed to participate in axonal degeneration (6, 12), its involvement in traumatic lesions in mammals in vivo has not yet been shown. Here we visualize the kinetics of axotomy-induced $[Ca^{2+}]_i$ changes in the ON of a living rat. Previously, extracellular calcium has been found to be the source of increased $[Ca^{2+}]_i$ in an in vitro stretch injury model (32). Calcium-permeable AMPA receptors have been proposed to participate in calcium influx after traumatic injury (33) and blockage of CNS-specific L-type and T-type calcium channels has been shown to prevent secondary RGC death following partial axotomy (34). In our study, a mixture of calcium channel inhibitors (L-type, T-type, AMPA) completely prevents $[Ca^{2+}]_i$ increase after the ON lesion arguing in favor of the extracellular space as a calcium source and for channel-mediated calcium entry. We thus conclude that mechanical disruption of axonal integrity alone and the generation of “mechanopores” are insufficient to induce a $[Ca^{2+}]_i$ increase. Local application of the calcium ionophore dramatically enhanced axonal degradation processes, whereas application of a calcium channel inhibitor mix nearly prevented degeneration and resulted in an attenuation of autophagosome numbers. Downstream of calcium influx, fragmentation of microtubules due to activation of proteases of the proteasome (35) or calpain (9) were observed after axonal injury and NMDA-induced increase of $[Ca^{2+}]_i$ has been associated with the expression of the autophagy marker LC3 (36). Our studies on lesion-dependent LC3 expression now link the initial increase of $[Ca^{2+}]_i$ to a secondary increase in autophagy.

In conclusion, our data suggest that mechanical injury to the ON induces extracellular calcium entry to the axolemma via calcium channels, resulting in rapid $[Ca^{2+}]_i$ increase. This results in a secondary generation of autophagosomes that participate in axonal degradation. Both events thus represent promising targets for future therapeutic interventions in the treatment of axonal pathology in degenerative and traumatic CNS disorders.

Methods

Surgical Approach and Crush Lesion of the Optic Nerve. All animal studies were carried out according to the regulations of the local animal research council and legislation of the state of Lower Saxony. Adult female Wistar rats (250–350 g; Charles River) were used. Anesthesia was performed by i.p. injection of 2% xylazine (7 mg/kg body weight) and 10% ketamine (95 mg/kg body weight). The ON was accessed by an adapted retroorbital surgical access (19, 37). Before imaging, a surgical suture (Ethicon; 10-0 Ethilon) was fixed loosely around the ON to serve as a marker. For ON crush, the suture was tightly constricted leaving the knot on the nerve. For details see *SI Methods*.

Intravitreal Injections. Intravitreal injections were performed 2 weeks (AAV) or 2.5 h (OGB, 3-methyladenine, DMSO) before imaging using a Hamilton syringe (Hamilton; model 701, 26s gauge, removable needle). Injected substances: AAV(1/2).hSYN.dsRed (5 μ L; 1×10^8 i.u./ μ L), Oregon Green 488 BAPTA-1 (Molecular Probes; 3 μ L, 3.97 mM), 3-methyladenine in DMSO (Sigma-Aldrich; 4 μ L, 33.3 mM), DMSO 30% in H₂O (Applchem; 4 μ L of working solution). The viral vector with serotype 2 inverted terminal repeats (ITRs) containing a DsRed2N1 expression cassette was constructed as recently described (38). For details, see *SI Methods*.

Imaging of Axonal Degeneration. An adapted epifluorescence microscope (Zeiss; AxioPlan) with a water immersion objective (Achromplan 40 \times /0.80 W DIC III, working distance 3.6 mm) was used to visualize axons at the ON surface within \sim 400 μ m proximal or distal to the lesion. Z-stack images were acquired at standardized time points after the lesion and single images selected for further evaluation. For detailed information, see *SI Methods*.

Calcium Imaging. Three microliters of OGB-1 working solution was injected intravitreally 2.5 h before imaging. For calcium channel inhibitor experiments, a mixture of 100 μ M amiloride, 10 μ M amlodipin, and 1 mM NBQX (all Sigma-Aldrich) was applied topically to the ON 30 min before the crush lesion. For ionophore studies we applied A23187 (100 μ M in 2% DMSO; Sigma-Aldrich) 30 min before the crush on the ON and the solution was exchanged against regular Ringer solution after crush. For imaging of

intraaxonal calcium ($[Ca^{2+}]_i$) levels, a representative ROI (85 \pm 35 μ m from the lesion site) was selected. The fluorescence intensity of each ROI was normalized to the intensity quantified in the first postlesional image and set to an arbitrary fluorescence unit of 1. For details, see *SI Methods*.

Electron Microscopy. After transcardial perfusion with 3% glutaraldehyde at 30 min, 2 h, and 6 h after ON crush, tissue proximal and distal to the crush site was further processed for ultrathin sections (\sim 60 nm). Electron microscopic (Zeiss) images were further quantified using AnalySIS (Olympus) and Photoshop (Adobe) software. LC3 immunogold labeling: LC3 antibody (Santa Cruz) 1:50 overnight followed by a 1.4-nm gold-coupled anti-goat-antibody (Sigma). For technical details, see *SI Methods*.

Immunohistochemistry and Quantification of LC3- β 62 Punctae. Longitudinal ON sections were rehydrated, permeabilized, and blocked before application of the primary antibodies (4 $^{\circ}$ C for 24 h): LC3 (goat; 1:50; Santa Cruz), phosphorylated neurofilaments (Smi31; mouse; 1:1,000; Covance) and p62/SQSTM1 (rabbit, 1:2,000; Sigma-Aldrich). Secondary antibodies (1 h at room temperature): cy2-conjugated donkey anti-mouse IgG 1:500, cy3-conjugated donkey anti-rabbit IgG 1:500, cy3-conjugated donkey anti-goat IgG 1:250, cy5-conjugated donkey anti-goat IgG 1:1,000 (all Jackson Labs). For further details and quantification see *SI Methods*.

Statistics. All experiments were replicated and the number of animals/replications is given in the results part for each experiment. Data are shown as mean \pm SEM and were analyzed by ANOVA and two-tailed *t* test (KyPlot software). Differences were considered significant as stated in the text.

ACKNOWLEDGMENTS. We thank Elisabeth Barski and Brigitte Maruschak for expert technical assistance, Anton Lingor for the generation of schematic drawings of the imaging setup, and Ivana Gadjanski for helpful discussions. P.L. and M.B. are supported by the Deutsche Forschungsgemeinschaft (DFG) Research Center for Molecular Physiology of the Brain. P.L. was supported by a grant from the Wings For Life Spinal Cord Research Foundation, the Forschungsförderungsprogramm of the University Medicine Göttingen, and a grant from the DFG (Li 1308/3-1).

- Hagg T, Oudega M (2006) Degenerative and spontaneous regenerative processes after spinal cord injury. *J Neurotrauma* 23:264–280.
- Navarro X (2009) Chapter 27: Neural plasticity after nerve injury and regeneration. *Int Rev Neurobiol* 87:483–505.
- Orimo S, et al. (2008) Axonal alpha-synuclein aggregates herald centripetal degeneration of cardiac sympathetic nerve in Parkinson's disease. *Brain* 131:642–650.
- Fischer LR, et al. (2004) Amyotrophic lateral sclerosis is a distal axonopathy: Evidence in mice and man. *Exp Neurol* 185:232–240.
- Cavanagh JB (1964) The significance of the "dying back" process in experimental and human neurological disease. *Int Rev Exp Pathol* 3:219–267.
- Coleman M (2005) Axon degeneration mechanisms: Commonality amid diversity. *Nat Rev Neurosci* 6:889–898.
- Coleman MP, Perry VH (2002) Axon pathology in neurological disease: A neglected therapeutic target. *Trends Neurosci* 25:532–537.
- Li H, Li SH, Yu ZX, Shelbourne P, Li XJ (2001) Huntingtin aggregate-associated axonal degeneration is an early pathological event in Huntington's disease mice. *J Neurosci* 21:8473–8481.
- Kerschensteiner M, Schwab ME, Lichtman JW, Misgeld T (2005) In vivo imaging of axonal degeneration and regeneration in the injured spinal cord. *Nat Med* 11:572–577.
- George EB, Glass JD, Griffin JW (1995) Axotomy-induced axonal degeneration is mediated by calcium influx through ion-specific channels. *J Neurosci* 15:6445–6452.
- Stys PK (2005) General mechanisms of axonal damage and its prevention. *J Neurosci* 23:3–13.
- Ziv NE, Spira ME (1995) Axotomy induces a transient and localized elevation of the free intracellular calcium concentration to the millimolar range. *J Neurophysiol* 74:2625–2637.
- Martin KR, Klein RL, Quigley HA (2002) Gene delivery to the eye using adeno-associated viral vectors. *Methods* 28:267–275.
- Martin KR, Quigley HA (2004) Gene therapy for optic nerve disease. *Eye (Lond)* 18:1049–1055.
- Planchamp V, et al. (2008) BAG1 promotes axonal outgrowth and regeneration in vivo via Raf-1 and reduction of ROCK activity. *Brain* 131:2606–2619.
- Carelli V, Ross-Cisneros FN, Sadun AA (2004) Mitochondrial dysfunction as a cause of optic neuropathies. *Prog Retin Eye Res* 23:53–89.
- Kolbe S, et al. (2009) Optic nerve diffusion changes and atrophy jointly predict visual dysfunction after optic neuritis. *Neuroimage* 45:679–686.
- Rosignol S, Schwab M, Schwartz M, Fehlings MG (2007) Spinal cord injury: Time to move? *J Neurosci* 27:11782–11792.
- Lingor P, Koeberle P, Kügler S, Bähr M (2005) Down-regulation of apoptosis mediators by RNAi inhibits axotomy-induced retinal ganglion cell death in vivo. *Brain* 128:550–558.
- Lingor P, et al. (2007) Inhibition of Rho kinase (ROCK) increases neurite outgrowth on chondroitin sulphate proteoglycan in vitro and axonal regeneration in the adult optic nerve in vivo. *J Neurochem* 103:181–189.
- Bähr M, Lingor P (2006) Brain repair: Experimental treatment strategies, neuroprotective and repair strategies in the lesioned adult CNS. *Adv Exp Med Biol* 557:148–163.
- Schlaepfer WW (1977) Structural alterations of peripheral nerve induced by the calcium ionophore A23187. *Brain Res* 136:1–9.
- Berkelaar M, Clarke DB, Wang YC, Bray GM, Aguayo AJ (1994) Axotomy results in delayed death and apoptosis of retinal ganglion cells in adult rats. *J Neurosci* 14:4368–4374.
- Pettus EH, Povlishock JT (1996) Characterization of a distinct set of intra-axonal ultrastructural changes associated with traumatically induced alteration in axolemmal permeability. *Brain Res* 722:1–11.
- Smith PM, Jeffery ND (2006) Histological and ultrastructural analysis of white matter damage after naturally-occurring spinal cord injury. *Brain Pathol* 16:99–109.
- Nixon RA (2006) Autophagy in neurodegenerative disease: Friend, foe or turncoat? *Trends Neurosci* 29:528–535.
- Rubinsztein DC, et al. (2005) Autophagy and its possible roles in nervous system diseases, damage and repair. *Autophagy* 1:11–22.
- Wang QJ, et al. (2006) Induction of autophagy in axonal dystrophy and degeneration. *J Neurosci* 26:8057–8068.
- Komatsu M, et al. (2007) Essential role for autophagy protein Atg7 in the maintenance of axonal homeostasis and the prevention of axonal degeneration. *Proc Natl Acad Sci USA* 104:14489–14494.
- Weisenberg RC, Deery WJ (1981) The mechanism of calcium-induced microtubule disassembly. *Biochem Biophys Res Commun* 102:924–931.
- Job D, Fischer EH, Margolis RL (1981) Rapid disassembly of cold-stable microtubules by calmodulin. *Proc Natl Acad Sci USA* 78:4679–4682.
- Wolf JA, Stys PK, Lusardi T, Meaney D, Smith DH (2001) Traumatic axonal injury induces calcium influx modulated by tetrodotoxin-sensitive sodium channels. *J Neurosci* 21:1923–1930.
- Spaethling JM, Klein DM, Singh P, Meaney DF (2008) Calcium-permeable AMPA receptors appear in cortical neurons after traumatic mechanical injury and contribute to neuronal fate. *J Neurotrauma* 25:1207–1216.
- Fitzgerald M, et al. (2009) Secondary degeneration of the optic nerve following partial transection: The benefits of lomerizine. *Exp Neurol* 216:219–230.
- Zhai Q, et al. (2003) Involvement of the ubiquitin-proteasome system in the early stages of wallerian degeneration. *Neuron* 39:217–225.
- Calderó J, et al. (2007) Excitotoxic motoneuron disease in chick embryo evolves with autophagic neurodegeneration and deregulation of neuromuscular innervation. *J Neurosci Res* 85:2726–2740.
- Lingor P, et al. (2008) ROCK inhibition and CNTF interact on intrinsic signalling pathways and differentially regulate survival and regeneration in retinal ganglion cells. *Brain* 131:250–263.
- Michel U, Malik I, Ebert S, Bähr M, Kügler S (2005) Long-term in vivo and in vitro AAV-2-mediated RNA interference in rat retinal ganglion cells and cultured primary neurons. *Biochem Biophys Res Commun* 326:307–312.